Available online at www.sciencedirect.com

ScienceDirect

journal homepage: www.elsevier.com/locate/issn/15375110

Research Paper

Control of a path following caterpillar robot based on a sliding mode variable structure algorithm

Zhiqiang Li [a], Liqing Chen [a,b,*], Quan Zheng [a,b], Xianyao Dou [a], Lu Yang [a]

[a] College of Engineering, Anhui Agricultural University, Hefei 230036, China
[b] Anhui Province Engineering Laboratory of Intelligent Agricultural Machinery and Equipment, Hefei 230036, China

ARTICLE INFO

Article history:
Received 12 March 2019
Received in revised form
24 June 2019
Accepted 22 July 2019
Published online 3 September 2019

Keywords:
Sliding mode variable structure control
Path following joint simulation
Tracked robot
Tall crops
Plant protection
Crop rows

Tracked plant protection robots operating in soft, sticky soil and complex environments such as during the middle and late stages of maize cultivation can deviate significantly from their desired path. A path following control algorithm of for a tracked robot based on a sliding mode variable structure algorithm and the control system was developed. A dynamic model of the interaction between tracked chassis and soil underneath using specific fluctuation characteristics and soft soil conditions was established using multi-body dynamic simulation software. The control system was developed in MATLAB/Simulink and a joint simulation test is carried out. The simulation results show that the sliding mode variable structure algorithm could achieve better control. Field tests were carried out and the results showed that the maximum path deviation for the tracked robot using control based the algorithm was 70 mm, and the average path deviation was 30 mm. There were no out-of-control phenomena. The robot was able to carry out effective late season plant protection operations among the maize rows realising human-machine separation and environmental prevention and control.

1. Introduction

Maize is an important food crop and feed source in China. Diseases and insect pests occur frequently in the middle and late stages of maize cultivation. The control of diseases and insect pests in the middle and late stages of maize growth effectively determines the yield of maize. Because of the high plant height and narrow row spacing during the middle and later stages of maize growth, large-scale high-clearance sprayers that demand a lot of energy and cause damage to the crop and soil, or applications with manual sprayers, where operator contamination is a risk, are used (Chen, Wang, Zhang, Zheng, & Wang, 2018). Small self-propelled plant protection robots for use in the middle and later stages of cultivation appear to be a more acceptable solution. However, the standard wheeled robot has some problems, such as small contact area, poor obstacle surmounting ability, poor topographic adaptability, and large turning diameter. It cannot perform well in the middle and late stages of maize plant protection. Tracked robots have high manoeuvrability, cross-country performance and flexibility, strong environmental adaptability and can have suitable carrying capacity. Because of the complex and harsh environment in agriculture, tracked

* *Corresponding author*. College of Engineering, Anhui Agricultural University, Hefei 230036, China.
E-mail address: lqchen@ahau.edu.cn (L. Chen).
https://doi.org/10.1016/j.biosystemseng.2019.07.004
1537-5110/

Nomenclature

Symbol

x_d	X-axis coordinates of any point in an ideal path, mm
y_d	Y-axis coordinates of any point in an ideal path, mm
θ_d	Angle between the ideal direction of the robot and the x-axis, rad
θ	Angle between the robot forward direction and the x-axis, rad
V	Linear speed of robot forward direction, mm s^{-1}
ω	Angular speed of robot rotating around centroid, rad s^{-1}
B	Track spacing, mm
L	Track shoe length, mm
v_x	X-axis direction velocity of robot, mm s^{-1}
v_y	Y-axis direction velocity of robot, mm s^{-1}
F_{x1}, F_{x2}	Longitudinal force on track, N
F_{y1}, F_{y2}	Lateral force on track, N
F_1, F_2	Shear force on track plate, N
v_1, v_2	Sliding speed of trackpad at any point during steering, mm s^{-1}
r_1, r_2	Distance from any point to geometric centre during steering, mm
x_1, x_2	X-axis abscissa of any point of trackpad
m	Robot mass, kg
O	Instantaneous steering centre
O'	Geometric centre
M_μ	Steering resistance moment, N m
I	Moment of inertia around the centre of mass, kg m^2
f	Track rolling friction factor
φ	Track and ground adhesion coefficient
g	gravity acceleration, m s^{-2}
R	Robot steering radius, mm
μ	Steering resistance coefficient
μ_{max}	Maximum steering resistance coefficient
F_L, F_R	Track driving force, N
R_L, R_R	Track driving Resistance, N
ω_1, ω_2	Angular speed of left and right driving motor, rad s^{-1}
η	Transmission efficiency
i	Transmission ratio
r	Driving wheel radius, mm
p_e	Rated power of driving motor, J s^{-1}
G	Robot weight, N
F_{fli}	Friction between load-bearing wheel and track, N
N_i	Load-bearing wheels are subjected to the reaction of track, N
F_r	Crawler preload, N
Z_0	Ground subsidence of the whole machine, mm
k_c	Modulus of cohesion of soil deformation
$k_\varnothing$	Internal friction modulus of soil deformation
b	Load plate width, mm
z_0	Soil subsidence, mm
n	Soil deformation index
j	Soil shear displacement, mm
k	Horizontal shear modulus of soil
A	Unit area of track contact ground
τ_m	Soil shear strength, Pa
τ	Shear stress, Pa
p	Compressive stress, Pa
$\varnothing$	Internal friction angle of soil
c	Soil cohesion
δ_1, δ_2	Angle between sliding velocity at any point of track grounding section and x-axis direction, rad
τ_L, τ_R	Shear force per unit area of track, Pa
p_L, p_R	Pressure on track unit area, Pa
ω_L, ω_R	Angular speed of driving wheel, rad s^{-1}
I_t	Track joint distance, mm
Z_K	Number of effective meshing teeth on driving wheel

Abbreviations

SMC	Sliding Mode Variable Structure Control
PID	Proportional Integral Differential
UKF	Unscented Kalman Filter
SMO	Sliding Mode Observer
DOF	Degree Of Freedom

robots are often more suitable than wheeled robots (Kayacan, Young, Peschel, & Chowdhary, 2018). Therefore, the research on tracked agricultural robots is becoming more and more extensive. For example a self-propelled thermal fogger chassis was proposed to solve the problems of difficult plant protection during the middle and late period of maize cultivation (Chen, Wang, Zhang, Zheng, & Wang, 2018). Multi stroke simultaneous operation of a tracked agricultural robot was realised because the hardware and software platform of tracked agricultural chemical dust removal robot based on XP embedded system was designed (Xian et al., 2012), It is also difficult to measure the sliding parameters of a tracked robot agricultural when it is running in complex environment, but with the development of sliding parameter estimation methods based on unscented Kalman filter (UKF) and sliding mode observer (SMO), the problem of tracking robots in complex environments can be solved (Jiao, Kong, Gu, Wang, Gao & Yuan, 2015).

Due to the unknown traction coefficient of track, complex soil conditions, the lack of coincidence between the geometric centre and the centre of mass (Jiao, Chen, Qiao, Wang, Wang, Gu & Li, 2018) and other field factors, tracked robots deviate from their predetermined trajectory and this may lead to crop damage and robot failure.

Accurate driving between crop rows to avoid damage is one of the most important tasks of agricultural robots during various field operations (such as monitoring, mechanical weeding or spraying pesticides). Therefore, much research has been carried out developing robot path tracking control algorithms, among which the proportional integral

differential (PID) control algorithm is the most widely used. For example, an adaptive robust hybrid control method based on multi-objective genetic algorithm optimization combined with sliding control was proposed (Taherkhorsandi, Mahmoodabadi, Talebipour, & Castillo-Villar, 2015). A fuzzy control algorithm which combines proportional, integral and differential algorithm with model predictive control algorithm has been developed (Wen, Chen, Qin, Zhu, & Wang, 2018) and a novel four-rotor proportional-integral-differential motion controller has been proposed (Moreno-Valenzuela,Perez-Alcocer, Guerrero-Medina & Dzul, 2018). The trajectory of this closed-loop system was analysed and the gain adjustment criteria were discussed. PID control algorithms are also commonly used in deep-sea mining robots, firefighting robots, forestry patrol robots and battlefield reconnaissance robots.

However, tracked agricultural robots have complex track-ground contact surfaces, and there are different trajectories between the tracks of tracked agricultural robots, which greatly increases the difficulty of path tracking (Kayacan, Young, Peschel & Chowdhary, 2018). When using standard control methods (such as PID control), path tracking performance will be degraded due to the existence of time-varying parameters (Fukao, Nakagawa, & Adachi, 2000). This is because the standard control algorithm cannot adjust the control parameters according to the soil parameters of an unknown terrain, and these parameters play an important role in determining the speed and steering of the robot (Kayacan, Ramon & Saeys, 2012), a agricultural crawler robot is a multi-input and multi-output system, and has the characteristic of time-varying, coupling, non-linearity and uncertainty (Kayacan, Young, Peschel, & Chowdhary, 2018). When dealing with extremely complex and unpredictable tasks, both on large and small spatial scales, there are extremely variable working conditions (Oberti & Shapiro, 2016). Due to the uncertainty and variability caused by parameter disturbance to the control model of the robot, performance of the conventional PID control algorithm is not particularly good (Jiang et al., 2018). Comparing the performance of different control algorithms such as PID, fuzzy control and neural control, it has been shown that standard or individual intelligent control methods are not suitable for tracked robots (Dai, Zhu, Zhou, Mao & Wu, 2018). The sliding mode variable structure control (SMC) algorithm can adjust time-based uncertainties, and parameter disturbances in a controlled system. Under the influence of external disturbances and uncertainties, SMC can reliably track the desired time-varying trajectory (Rios, Falcon & Gonzalez, 2019) in an exponential convergent manner, and improve the fault tolerance of the control process (Huang, Naghdy, & Du, 2019). Compared with the PID control algorithm, it can improve the robustness of the system (Fan, Zhang, Wang, & Zhou, 2018). The SMC algorithm is therefore capable of path tracking tracked robots in complex field environments. Based on the previous research, this paper designs path tracking control algorithm, based on SMC algorithm, which is suitable for use by a tracked robot operating in maize and carrying out plant protection operations.

2. Robot modelling

2.1. Mathematical model of robot

The driving wheels on both sides of a tracked plant protection robot are driven independently by the electric motors on both sides. A 3 degrees of freedom (DOF) model for a tracked plant protection robot was established based on Fig. 1. It includes a longitudinal motion around the X-axis, the lateral motion around Y-axis and yaw motion around Z-axis. In the process of modelling, the following simplifications were made for the tracked plant protection robot.

(1) The origin of the moving coordinate system coincides with the centroid of the robot;
(2) Ignoring the suspension, the robot only moves parallel to the ground;
(3) Ignoring the influence of steering system, the mechanical characteristics of the two tracks are the same.

The simplified dynamics model of tracked plant protection robot are shown in Fig. 1. In the picture O is Instantaneous steering centre;O' is Geometric centre. R is Robot steering radius, mm.

From Fig. 1, the dynamic equations of tracked robot are described as

$$\begin{cases} m\dot{v}_x = (F_L + F_R)\cos\theta + (F_{x1} + F_{x2})\cos\theta - (F_{y1} + F_{y2})\sin\theta - (R_L + R_R)\cos\theta \\ m\dot{v}_y = (F_L + F_R)\sin\theta + (F_{x1} + F_{x2})\sin\theta - (F_{y1} + F_{y2})\cos\theta - (R_L + R_R)\sin\theta \\ I\dot{\omega} = (F_R + F_{x2} - F_{x1} + R_L - R_R)\dfrac{B}{2} - M_\mu \\ M_\mu = \mu mgL/4 \\ v_x = V\cos\theta \\ v_y = V\sin\theta \\ R_R = R_L = mgf/2 \\ \mu = \mu_{max}/(0.925 + 0.15R/B) \\ \max(F_L, F_R) \le \varphi mg/2 \end{cases} \quad (1)$$

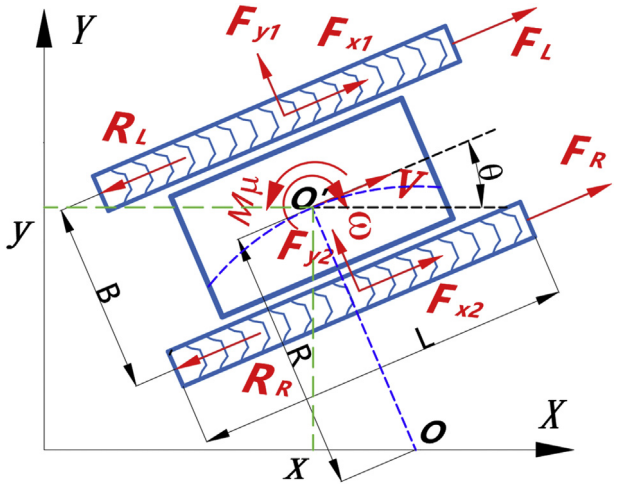

Fig. 1 – Tracked robot model.

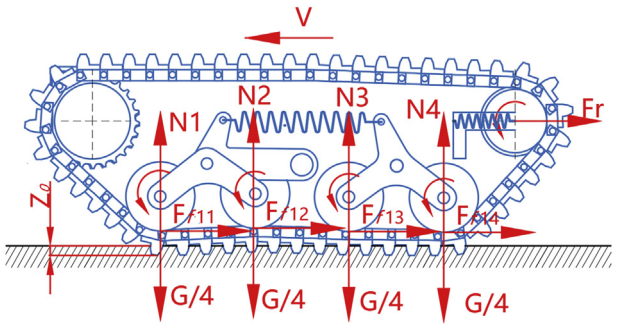

Fig. 2 – Force diagram of tracked robot.

where φ is track and ground adhesion coefficient; m is Robot mass, kg; v_x is X-axis direction velocity of robot, mm s^{-1};v_y is Y-axis direction velocity of robot, mm s^{-1}; F_L,F_R is Track driving force, N; F_{x1},F_{x2} is Longitudinal force on track, N; F_{y1},F_{y2} is Lateral force on track, N; θ is Angle between the robot forward direction and the x-axis, rad; R_L,R_R is Track driving Resistance, N; ω is Angular speed of robot rotating around centroid, rad s^{-1}; I is Moment of inertia around the centre of mass, kg m^2; B is Track spacing, mm; M_μ is Steering resistance moment, N m; μ is Steering resistance coefficient; L is Track shoe length, mm; V is Linear speed of robot forward direction, mm s^{-1}; f is Track rolling friction factor; μ_{max} is Maximum steering resistance coefficient;g is gravity acceleration, m s^{-2}.

The driving force of the track on the left and right sides are expressed as follows:

$$\begin{cases} F_R = 1946 p_e \pi \eta i / \omega_2 r \\ F_L = 1946 p_e \pi \eta i / \omega_1 r \end{cases} \tag{2}$$

where p_e is Rated power of driving motor, J s^{-1}; η is Transmission efficiency; i is Transmission ratio; r is Driving wheel radius, mm; ω_1,ω_2 is Angular speed of left and right driving motor, rad s^{-1}.

2.2. *Track-soil interaction*

The working environment of tracked robot described in this paper is a soft soil such as the *Shajiang* black soil. The overall forces acting on the tracked robot are shown in Fig. 2. In the picture G is Robot weight, N; F_{fli} is Friction between load-bearing wheel and track, N; N_i is Load-bearing wheels are subjected to the reaction of track, N; F_r is Crawler preload, N.

The positive pressure between track and ground satisfies the pressure-subsidence relationship proposed by Bekker (Chen, Wang,Zhang, Zheng,&Wang, 2018).

$$p = \left(\frac{k_c}{b} + k_\varnothing\right) z_0^n \tag{3}$$

where p is Compressive stress, Pa; z_0 is Soil subsidence, mm; k_c is Modulus of cohesion of soil deformation; $k_\varnothing$ is Internal friction modulus of soil deformation; Z_0 is Ground subsidence of the whole machine, mm; b is Load plate width, mm; n is Soil deformation index.

The relationship between the shear stress of track and the soil deformation satisfies the formula of shear stress and deformation proposed by Janosi (Zhu,Wang, Tian,Zhang&Chen, 2012).

$$\tau = \tau_m \left(1 - e^{-\frac{j}{k}}\right) \tag{4}$$

$$\tau_m = c + p \tan \varnothing \tag{5}$$

where j is Soil shear displacement, mm; k is Horizontal shear modulus of soil; τ_m is Soil shear strength, Pa; ∅ is Internal friction angle of soil; c is Soil cohesion; τ is shear stress, Pa.

Therefore, the shear stress between the left and right track and the ground can be expressed as

$$\begin{cases} \tau_L = (c + p_L \tan \varnothing)\left(1 - e^{-\frac{j}{k}}\right) \\ \tau_R = (c + p_R \tan \varnothing)\left(1 - e^{-\frac{j}{k}}\right) \end{cases} \tag{6}$$

where τ_L,τ_R is Shear force per unit area of track, Pa; p_L, p_R is Pressure on track unit area, Pa.

On the soft ground, the shear force between the track and the ground is opposite to the sliding velocity direction of the track, as shown in Fig. 3. In the picture v_1, v_2 is Sliding speed of trackpad at any point during steering, mm s^{-1}; r_1,r_2 is Distance from any point to geometric centre during steering, mm.

According to Eq. (6), the shear force acting on the grounding section of the track on both sides can be described as follows

$$\begin{cases} dF_1 = \tau_L dA = (c + p_L \tan \varnothing)\left(1 - e^{-\frac{j}{k}}\right) dA \\ dF_2 = \tau_R dA = (c + p_R \tan \varnothing)\left(1 - e^{-\frac{j}{k}}\right) dA \end{cases} \tag{7}$$

where F_1,F_2 is Shear force on track plate, N; A is unit area of track contact ground.

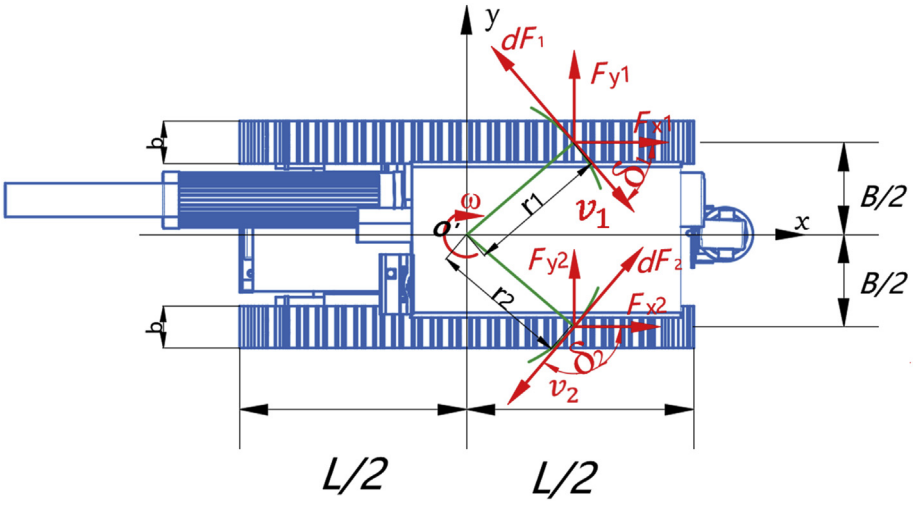

Fig. 3 – Diagram of track steering dynamics on both sides.

From to Eq. (7), the longitudinal force acting on both sides of the track are as follows

$$\begin{cases} F_{y2} = b\int_{\frac{-L}{2}}^{\frac{L}{2}} (c + p_R \tan\varnothing)\left(1 - e^{-\frac{j}{k}}\right)\cos(\pi - \delta_2)dx \\ F_{y1} = b\int_{\frac{-L}{2}}^{\frac{L}{2}} (c + p_L \tan\varnothing)\left(1 - e^{-\frac{j}{k}}\right)\cos(\delta_1)dx \end{cases} \tag{8}$$

where, δ_1, δ_2 is Angle between sliding velocity at any point of track grounding section and x-axis direction, rad.

The lateral force acting on both sides of the track is as follows

$$\begin{cases} F_{x2} = b\int_{\frac{-L}{2}}^{\frac{L}{2}} (c + p_R \tan\varnothing)\left(1 - e^{-\frac{j}{k}}\right)\sin(\pi - \delta_2)dx \\ F_{x1} = -b\int_{\frac{-L}{2}}^{\frac{L}{2}} (c + p_L \tan\varnothing)\left(1 - e^{-\frac{j}{k}}\right)\sin(\delta_1)dx \end{cases} \tag{9}$$

$$\cos(\delta_1) = \frac{{x_1}^{1/2}}{\left({x_1}^2 + (B/2)^2\right)^{1/2}} \tag{10}$$

$$\cos(\pi - \delta_2) = \frac{{x_2}^{1/2}}{\left({x_2}^2 + (B/2)^2\right)^{1/2}} \tag{11}$$

where x_1, x_2 is X-axis abscissa of any point of trackpad.

3. Design of path following control strategy for robots

3.1. Position control law design

The state of the tracked robot is represented by the position of the central point of the axis in the coordinate system and the heading angle θ, as shown in Fig. 1. The ideal trajectory is (x_d y_d), the ideal heading angle is θ_d, as shown in Fig. 4. In the picture $\mathbf{x_d}$ is X-axis coordinates of any point in an ideal path, mm; $\mathbf{y_d}$ is Y-axis coordinates of any point in an ideal path, mm; θ_d is Angle between the ideal direction of the robot and the x-axis, rad.

Firstly, x-tracking x_d and y-tracking y_d are realised by designing a position control rate v. Then the error tracking equation is as follows:

$$\left\{ \dot{x}_e v\cos\theta - \dot{x}_d\dot{y}_e = v\sin\theta - \dot{y}_d \right. \tag{12}$$

where $x_e = x - x_d$, $y_e = y - y_d$, take

$$\begin{cases} v\cos\theta = u_1 \\ v\sin\theta = u_2 \end{cases} \tag{13}$$

For $\dot{x}_e = v\cos\theta - \dot{x}_d$, if the sliding mode function is $s_1 = x_e$, then

$$\dot{s}_1 = \dot{x}_e = u_1 - \dot{x}_d \tag{14}$$

Design control rate is as follows

$$u_1 = \dot{x}_d - k_1 s_1 \tag{15}$$

where $k_1 > 0$, Take. $k_1 = 0.3$

So $\dot{s}_1 = -k_1 s_1$, take $V_x = \frac{1}{2}{s_1}^2$, $\dot{V}_x = s_1\dot{s}_1 = -k_1{s_1}^2$, that is $\dot{V}_x = -2k_1 V_x$, so that the x_e index converges to zero.

For $\dot{y}_e = v\sin\theta - \dot{y}_d$, if the sliding mode function is $s_2 = y_e$, then

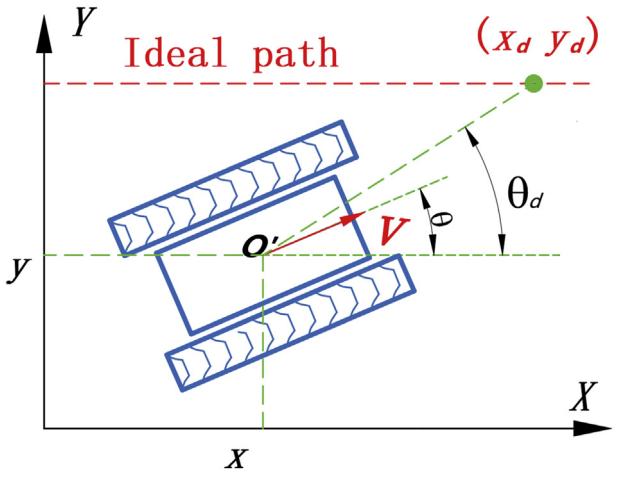

Fig. 4 – Path following diagram.

$$\dot{s}_2 = \dot{y}_e = u_2 - \dot{y}_d \tag{16}$$

Design control rate is as follows

$$u_2 = \dot{y}_d - k_2 s_2 \tag{17}$$

where $k_2 > 0$, Take $k_2 = 0.3$

So $\dot{s}_2 = -k_2 s_2$, take $V_y = \frac{1}{2}s_2^2$,$\dot{V}_y = s_2\dot{s}_2 = -k_2 s_2^2$, that is $\dot{V}_y = -2k_2 V_y$, so that the y_e index converges to zero.

From Eq. (14), $\frac{u_2}{u_1} = \tan\theta$ can be obtained, if the range of θ is $(-\pi/2\ ,\ \pi/2)$, θ satisfies the requirement of ideal trajectory tracking.

$$\theta = \arctan\frac{u_2}{u_1} \tag{18}$$

θ obtained by Eq. (14) is the angle required by position control law Eqs. (15) and (17), if θ and θ_d are equal, the ideal trajectory control law Eqs. (15) and (17) can be realised. However, θ and θ_d in the model is not completely consistent, especially in the initial stages of control and this will cause instability in the closed-loop tracking system.

Therefore, it is necessary to take the angle theta obtained by Eq. (18) as the ideal value, by using

$$\theta_d = \arctan\frac{u_2}{u_1} \tag{19}$$

When designing an ideal pose instruction $[x_d\ y_d]$, it is necessary to satisfy the range of θ_d $(-\pi/2\ ,\ \pi/2)$.

From Eq. (15), the actual position control law can be obtained as follows:

$$v = \frac{u_1}{\cos\theta_d} \tag{20}$$

The difference between actual θ and θ_d will result in the inaccurate realization of position control law Eqs. (15) and (17). The solution adopted in this paper is to design attitude control algorithm which converges faster than position control law so that θ can track θ_d as soon as possible.

3.2. Attitude control law design

By designing an attitude control law ω_θ, angle θ tracking θ_d are realised.

If $\theta_e = \theta - \theta_d$, and the sliding mode function is $s_3 = \theta_e$, then

$$\dot{s}_3 = \dot{\theta}_e = \omega_\theta - \dot{\theta}_d \tag{21}$$

The attitude control law is designed as follows

$$\omega_\theta = \dot{\theta}_d - k_3 s_3 - \eta_3 sgns_3 \tag{22}$$

where $k_3 > 0, \eta_3 > 0$, Take $k_3 = 3$, $\eta_3 = 0.5$.

Then $\dot{s}_3 = -k_3 s_3 - \eta_3 sgns_3$, take $V_\theta = \frac{1}{2}s_3^2$, $\dot{V}_\theta = s_3\dot{s}_3 = -k_3 s_3^2 - \eta_3|s_3| \le -k_3 s_3^2$, that is $\dot{V}_\theta \le -2k_3 V_\theta$, so the angle θ exponent converges to θ_d.

3.3. Design of signal converter

The output signals of the controller are the linear velocity Vand the angular velocity ω of the tracked robot. While the actual inputs of the tracked robot are the angular velocities ω_1 and ω_2 of the left and right tracked drive motor, this make $V = v$, $\omega = \omega_\theta$. So, the signal converter was designed as follows.

$$\begin{cases} \omega_\theta\left(R + \dfrac{B}{2}\right) = V_L \\ \omega_\theta\left(R - \dfrac{B}{2}\right) = V_R \\ \omega_\theta R = v \end{cases} \tag{23}$$

It can be obtained from Eq. (22).

$$\begin{cases} v + \dfrac{\omega_\theta B}{2} = V_L = Z_K I_t \omega_L / 2\pi \\ v - \dfrac{\omega_\theta B}{2} = V_R = Z_K I_t \omega_R / 2\pi \end{cases} \tag{24}$$

$$\begin{cases} \omega_1 i\eta = \omega_L \\ \omega_2 i\eta = \omega_R \end{cases} \tag{25}$$

where ω_L, ω_R is Angular speed of driving wheel, rad s^{-1}; I_t is Track joint distance, mm; Z_K is Number of effective meshing teeth on driving wheel.

The signal converter is designed as follows

$$\begin{cases} \omega_1 = \left(v + \dfrac{\omega_\theta B}{2}\right) 2\pi / Z_K I_t i\eta \\ \omega_2 = \left(v - \dfrac{\omega_\theta B}{2}\right) 2\pi / Z_K I_t i\eta \end{cases} \tag{26}$$

Therefore, through active control of ω_1 and ω_2 , the travelling state of the tracked robot can be controlled. The control strategy diagram based on SMC is shown in Fig. 5.

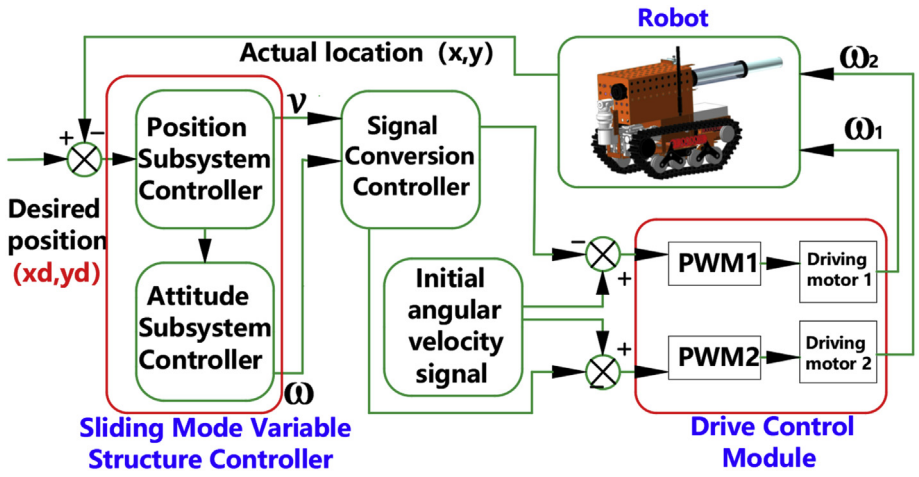

Fig. 5 – Sliding mode variable structure control strategy.

4. Joint simulation of path-following control

4.1. *Simulation model*

4.1.1. *Multi-body dynamics model of robot*

A multi-body dynamic model of experimental tracked robot was established by using RecurDyn/Track, a dynamic simulation program based on relative coordinate system and relative recursive algorithm. As shown in Fig. 6, the tracked plant protection robot is a complex mechanical system. In order to highlight the performance analysis of the robot's motion system, the simulation model was simplified as follows:

1) The working parts were assumed to be rigid bodies;
2) Some rigid unimportant parts, such as nuts and bolts were omitted; moving parts of the were included.;
3) The model parameters were obtained by three-dimensional measurement, calculation or experiment.

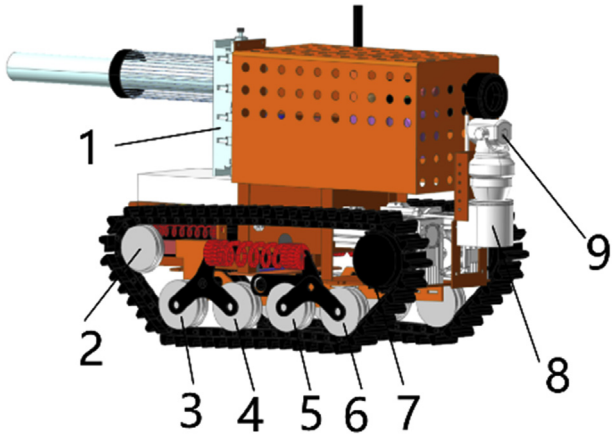

Fig. 6 – Three-dimensional multi-body dynamic model of tracked robot.

4.1.2. *Soil simulation model*

The software RecurDyn (Recursive Dynamic) V9R2, a multi-body system dynamics simulation software developed by FunctionBay Company, Korea, was used. It provided the setting of ground parameters. The undulating profile of the pavement (soil) was established using spline curves. After closure, the road surface is divided into rectangular units. The simulated ground information was acquired by the author Zhiqiang Li from the real inter line information acquired from the experimental field in Suzhou City, Anhui Province, China. The acquisition data was obtained by using VLP-16 three-dimensional terrain scanning radar (Velodyne LiDAR, Inc, CA, USA).

The scanning results are shown in Fig. 7a. The simulated ground environment was therefore very similar to the real environment. The average undulation data of the soil surface

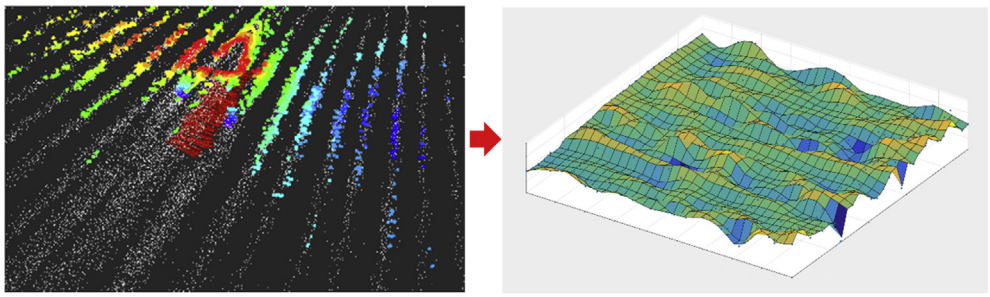

Fig. 7 – Soil surface treated by MATLAB. (a). Scanning results. (b) Processing results.

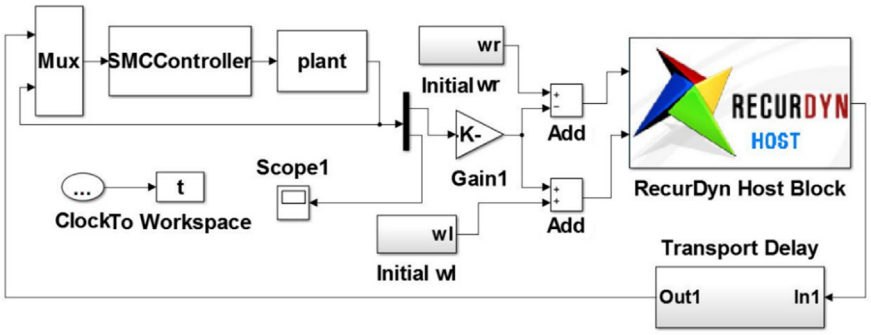

a Sliding mode variable structure control system diagram

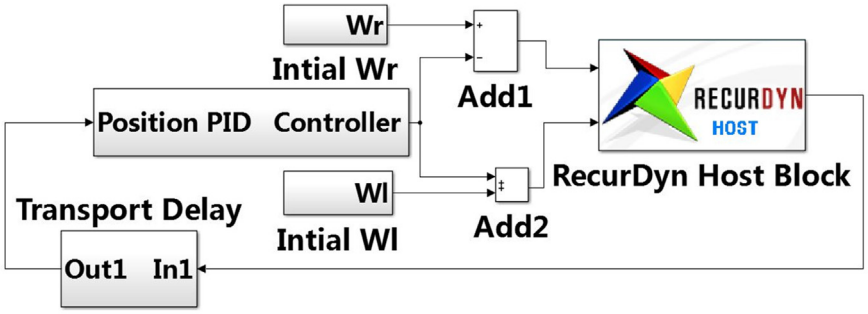

b Position based PID control system diagram

Fig. 8 – Control system diagram.

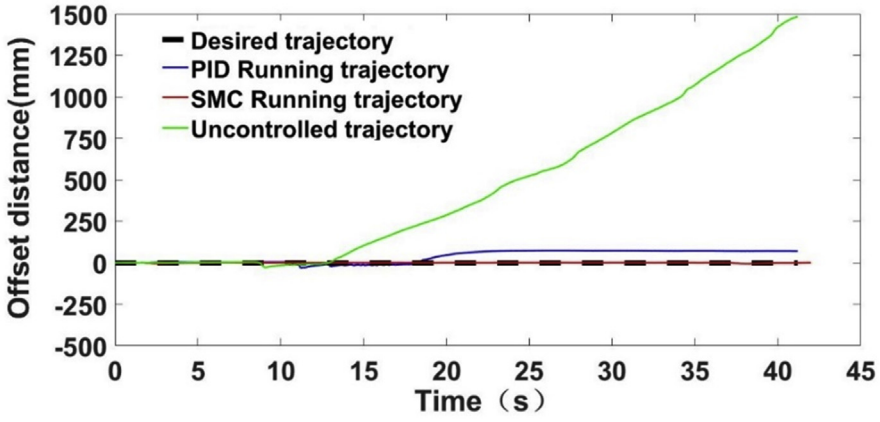

a simulation results

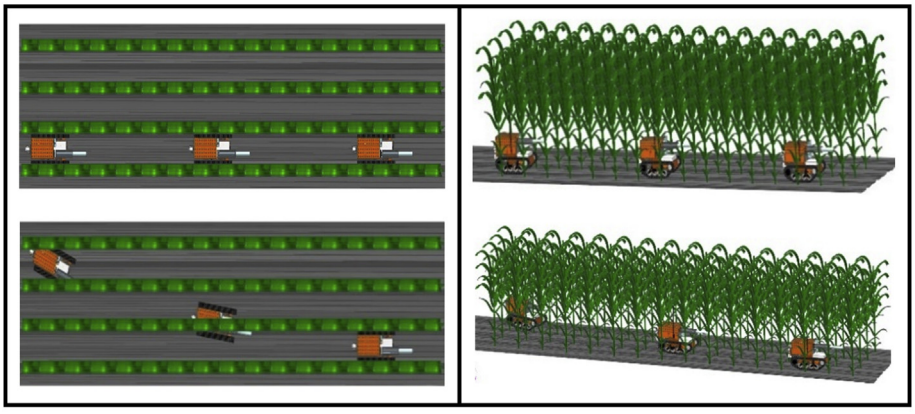

b Real-time simulation results

Fig. 9 – Simulation results.

was obtained by processing the data using MATLAB software version R2014b (MathWorks Company, USA)., as shown in Fig. 7b.

The obtained data were input into RecurDyn software to obtain the soil model, and then the contact data between soft ground and track were set up to complete the establishment of the ground simulation model.

4.2. *Joint simulation*

According to the designed control strategy and simulation model, the joint simulation was carried out by using RecurDyn and Simulink software. The input of the tracked robot was defined as the angular velocity ω_1 and ω_2 of the left and right motor, and the output is the actual coordinate position of the tracked robot. Through the combination of the joint simulation interface with the control system built in Simulink, a complete closed control loop is formed. According to the designed sliding mode variable structure control strategy, a SMC system is built in Simulink as shown in Fig. 8a, A position based PID control system was also built in Simulink as shown in Fig. 8b. In the PID control system, $k_p = 8$, $k_d = 0.1$, $k_i = 10$. The two control systems were then used for joint simulation.

The simulation environment was set as the complex field environment in the middle and late stages of maize cultivation. The simulation results are shown in Fig. 9. As can be seen in Fig. 9a, due to the uneven distribution of soil mechanical properties and the influence of other environmental factors, the trajectory deviated from the expected linear trajectory. With the increase of driving distance, the deviation continued to increase. According to the requirements for track deviation control of the robot, the deviation should be within the allowable range of − 100 mm to + 100 mm. The simulation results show that the tracked robot could not operate self-propelled plant protection in complex environment without a closed-loop control system.

The PID control algorithm could control the tracked robot along its desired path although at longer driving distances, it began to deviate from its desired path. The maximum deviation was 71.2 mm. Although this meets the path tracking requirements for a tracked robot in a complex field environment, the adaptability of the PID control algorithm to the variable environmental factors is very limited.

The tracked robot using an SMC system can accurately track the desired path, and as the distance increased the maximum offset of the robot was 5.7 mm. The simulation results show that the tracking effect of the crawler robot controlled by a sliding mode variable structure control algorithm is better than that achieved by PID control and the tracking response is faster.

4.3. *Robot path following stability analysis*

4.3.1. *Stability analysis of driving wheel*

The angular velocity curves of the left and right driving wheels of the tracked robot were obtained from data when the robot used the PID control algorithm and the SMC algorithm, as shown in Fig. 10, The angular acceleration curve of the left and

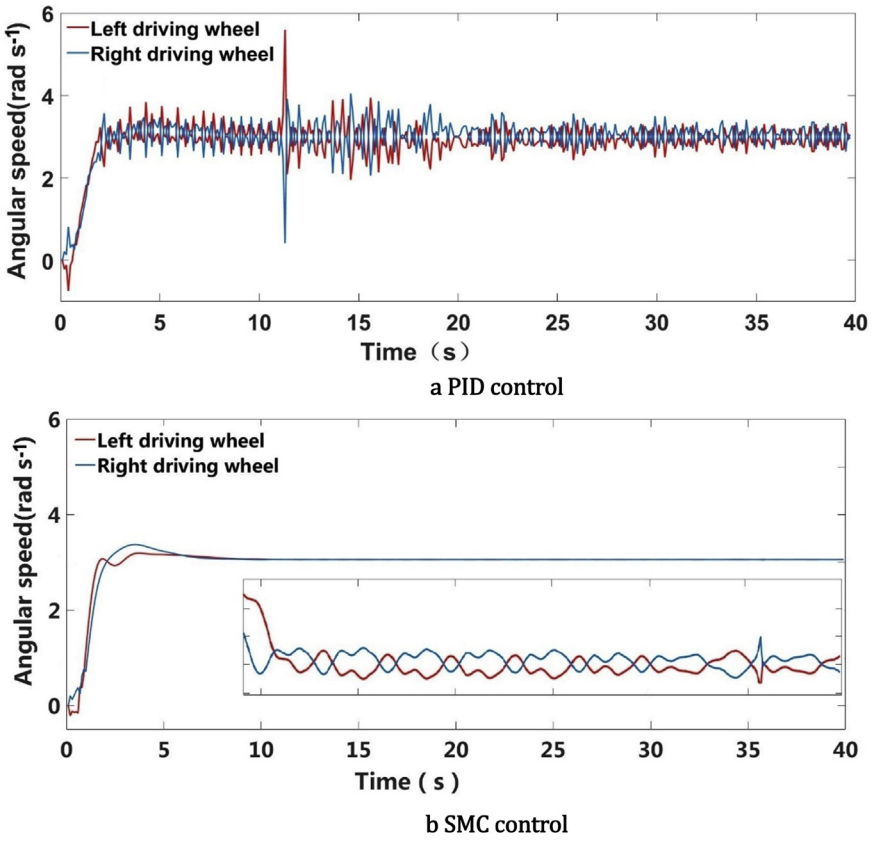

Fig. 10 – Angular Velocity Curve of a Driving Wheel Controlled by Different Algorithms.

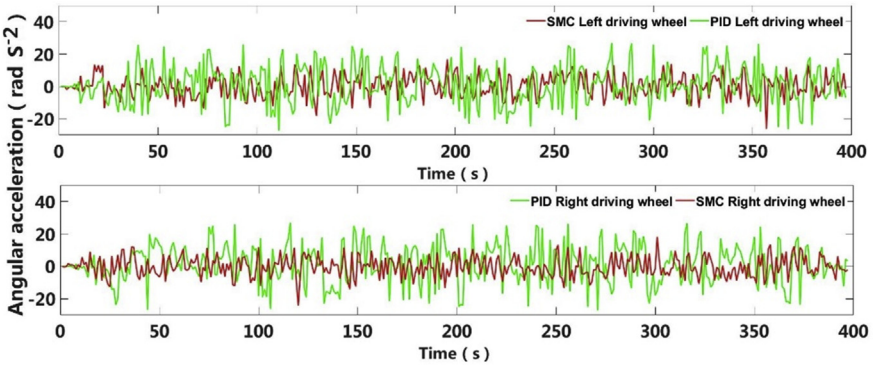

Fig. 11 – Angular acceleration curve of a driving wheel controlled by different algorithms.

right driving wheels of the tracked robot is shown in Fig. 11. Under the control of the PID algorithm, the angular velocity of the left and right driving wheels of the tracked robot varied in the range of -1 rad s^{-1} to + 1 rad s^{-1}, and the fluctuations were relatively large and stability was poor. This could have a great impact on the stability of the robot in a complex field environment, and the high frequency angular velocity changes could harm to the motor. When the SMC algorithm was adopted, the angular velocity of the left and right driving wheels of the robot changed smoothly and the angular acceleration of the driving wheel using the SMC control algorithm fluctuated less and was relatively stable. In the long-term, this should be very beneficial for field work.

4.3.2. *Overturning resistance of robots*

The travelling stability of a tracked robot is affected by its anti-overturning performance. Uncertain natural factors may occur at any time in complex field environment, such as on pavements with large undulations, large blocks of soil and on maize straw extending onto the road. Thus, crawler robots may appear to roll over or sway excessively. The changes of yaw angular velocity and pitch angular velocity for the crawler robot using the PID control algorithm and the SMC algorithm are shown in Fig. 12.

Figure 12 shows that the SMC algorithm can change purposefully according to the current state (such as deviation and its derivatives, etc.) in the dynamic process, and it is

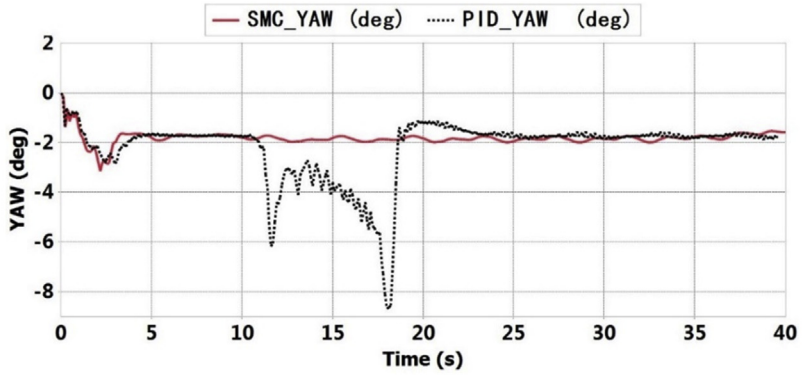

a Simulation Curves of Robot Yaw Angle Controlled by Different Control Algorithms

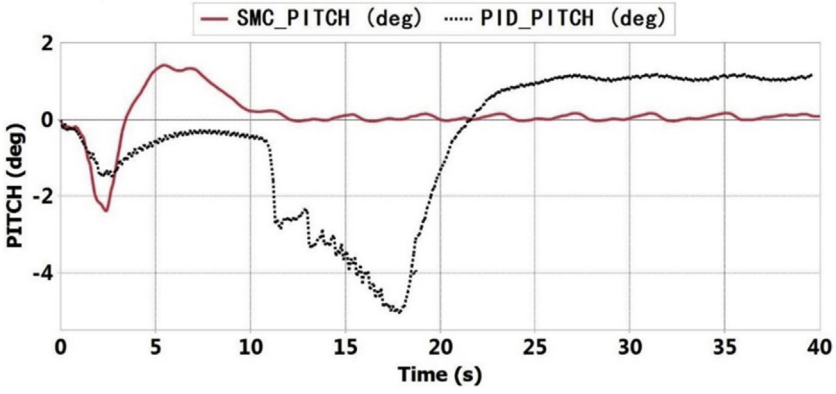

b Simulation Curve of Robot Pitch Angle Controlled by Different Control Algorithms

Fig. 12 – Overturning curve of robot under different control algorithms.

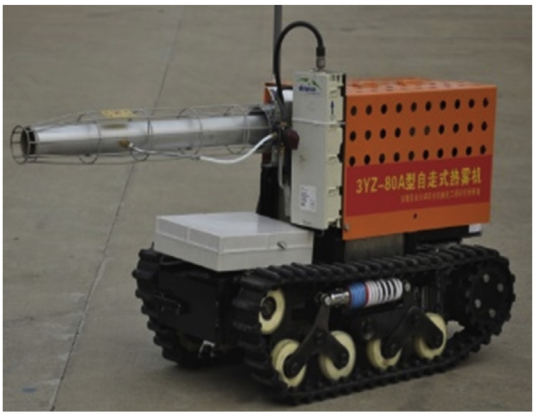

Fig. 13 – 3YZ-80A Material object map.

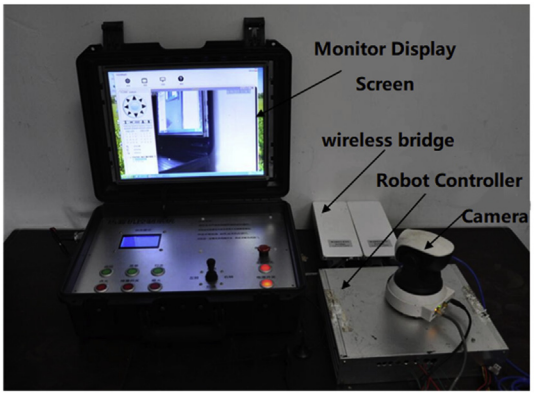

Fig. 14 – Network communication. Remote control system.

insensitive to disturbance. Thus, the sliding mode variable structure control system designed in this paper appeared to restrain the lateral and axial swings of the tracked robot well.

5. Field test verification

In order to verify the validity of the SMC algorithm proposed in this paper, it was tested on the 3YZ-80A tracked robot platform designed and developed by Anhui Intelligent Agricultural Machinery and Equipment Engineering Laboratory of Anhui Agricultural University, Hefei, China. The main components of the platform are shown in Fig. 13. In order to detect and avoid the collisions in the field during self-propelled operations, a remote-control system of network communication based on W5500 ethernet chip was installed in the controller of the robot, as shown in Fig. 14. It formed a local area network with the signal transmitted by wireless router and bridge. Using the camera installed on the robot, the movement of the robot was monitored in real time. When path deviation occurs the robot cannot track the path by autonomously but the manual remote control can ensure the robot continues operation.

During the experiment, the robot detected the inter-row environment of the maize crop using a LMS111-10100 laser radar scanning range finder (SICK AG, Waldkirch, Germany) installed in the front of the chassis, as shown in Fig. 15. After the laser sensor obtained the inter-row data from the maize plants, the controller processed it and fitted the ideal path of the robot, as shown by the green curve in Fig. 15. The controller adjusted the rotational speed of the left and right driving wheels of the robot according to the ideal path, so as to avoid collision of the robot between the rows of corn and in a position to carry out the plant protection operation.

5.1. *Simulated field environment test*

Before the experiment, the test site was set up mimicking the real environment between rows of maize. The transverse distance of maize plant model was 500 mm, and the longitudinal distance was 300 mm. Then the control program based on C++ is written into the controller. The microprocessor used in the controller is STM32F103ZGT6. After debugging, the robot was tested. Specific experimental methods are as follows: The robot tracked along a path between the set corn rows as shown in Fig. 16.

The offset distance of the robot was measured every 500 mm, and the experiments were repeated three times. The attitude data collected during the experiments by the laser radar scanning range finder was processed, and the results are shown in Fig. 17. The results show that the maximum offset distance of the robot during the simulated field environment was 30 mm and the average offset distance was 20 mm. Thus the robots could track the desired path. The maximum yaw angle and yaw velocity of the robot were 0.65° and 0.045° s^{-1} respectively. The range of pitch angular velocity and rolling

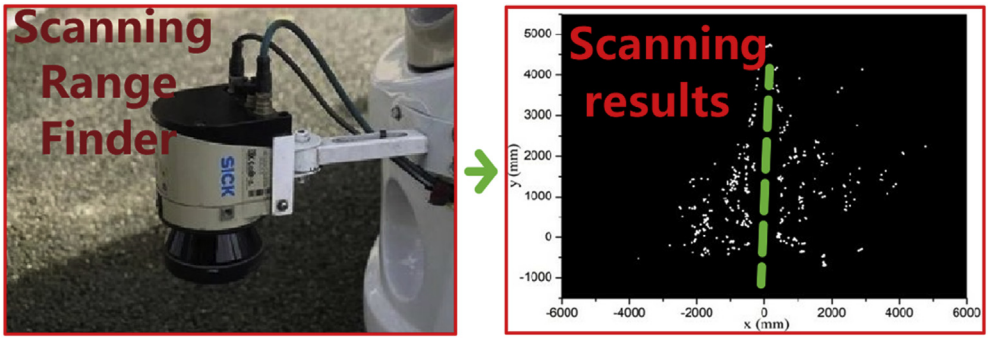

Fig. 15 – Ideal path acquisition diagram.

Fig. 16 – Simulated test site.

angular velocity was small, and the fluctuation range of the curve was gentle.

5.2. *Field driving offset test*

The real working environment of the robot is harsher and more complex than that of the simulation environment. At the same time, the mass of the robot was greater and the difficulty of control increased. Therefore, the offset distance relative to the desired path is one of the indicators that reflects control performance under real operating conditions.

The machine was filled with pesticide and a plant protection operation was carried out between the rows of maize with a width of 800 mm and a length of 500 m, as shown in Fig. 18. The offset distance between the robot and the desired path is measured every 10 m. Three experiments were repeated and the data recorded, as shown in Fig. 19.

Fig. 18 – Plant protection test site.

The experimental results show that for 500 m driving distance under a real field environment, the maximum and average deviation of the trajectory of the robot were 70 mm and 30 mm respectively, and no out-of-control phenomena occurred during the plant protection operation. In the complex field environment, the robot can be affected by many factors, which is why the offset distance was larger than during the test conducted in the simulated field environment. However, the robot met the requirements for plant protection in the middle and later stages of maize crop development.

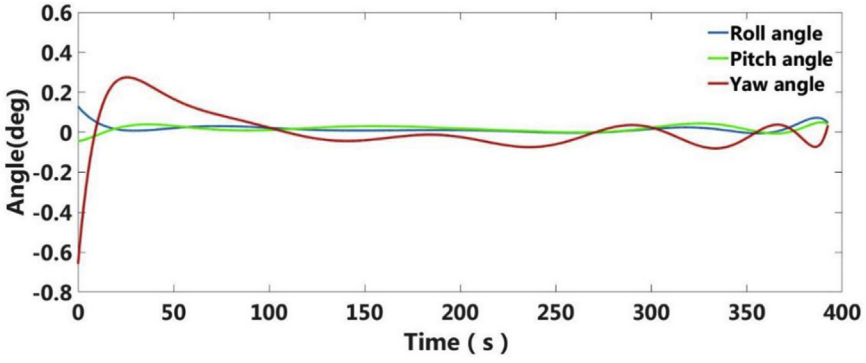

(a) Angle curve

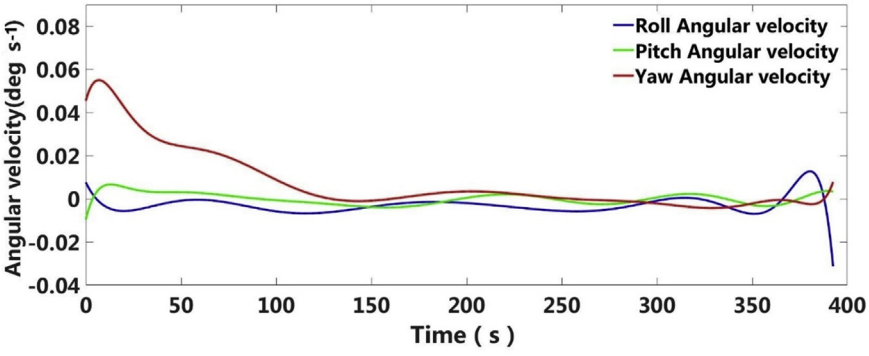

(b) Angular velocity curve

Fig. 17 – Robot driving attitude curve.

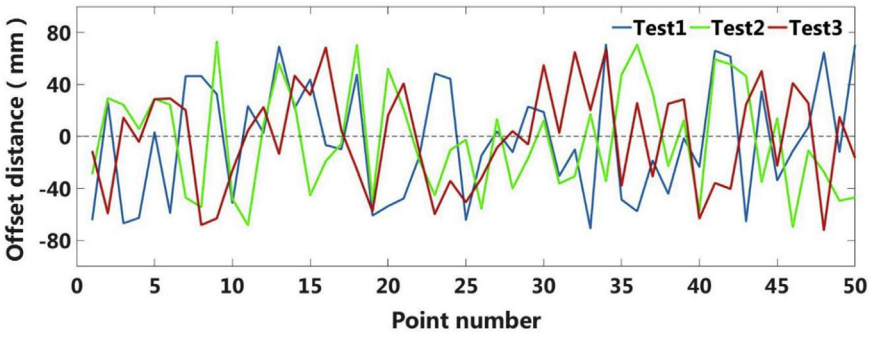

Fig. 19 – Offset distance curve.

6. Conclusions

A path following control algorithm based on SMC theory was proposed for controlling to route of a tracked agricultural robot designed for travelling between rows of maize crops and applying plant protection products. The standard PID control algorithm and the developed SMC algorithm were compared by simulation. Comparing the standard PID control algorithm with SMC algorithm by simulation, the feasibility and validity of SMC algorithm applied to a tracked agricultural robot was verified with the results showing that the maximum deviation of the trajectory using the PID control algorithm was 71.2 mm, and the maximum deviation of the robot trajectory using the SMC control algorithm was 5.7 mm. Field experiments were also conducted. The results showed that the tracked plant protection robot using an SMC control algorithm can track the desired path in the field, and the maximum deviation value of the path was 70 mm which meets the requirements for the inter-row plant protection in maize.

This work helps provides a new method for pest control in maize and other tall crops by realising man-machine separation and green prevention and control. It is hoped that this method will contribute to the development of agricultural robots.

7. Future work

The field experiment was carried out in August 2018, during the period for plant protection of summer maize in Anhui Province, China. Therefore, the experiment was mainly conducted among maize rows. This did not allow consideration of the behaviour of the robot under different initial conditions or conducting a comparative test between the SMC and PID control algorithms. This will be the subject of future experiments and research.

In this study, the pressure-subsidence formula and the shear stress formula were used to derive the control algorithm for conventional soils, but errors may occur when the two formulae are applied to maize inter-row soils which contain weeds and straw. This aspect should be investigated further.

Acknowledgment

This research is funded by China National Key Research and Development Program (2017YFD0301303), Natural Science Fund Project in Anhui Province (No. 1708085ME135) and Natural Science Major Project in Anhui Province (No. KJ2018ZD016).

REFERENCES

Chen, L. Q., Wang, P. P., Zhang, P., Zheng, Q., He, J., & Wang, Q. J. (2018). Performance analysis and test of a maize inter-row self-propelled thermal fogger chassis. *International Journal of Agricultural and Biological Engineering, 11*(5), 100–107.

Dai, Y., Zhu, X., Zhou, H., Mao, Z., & Wu, W. (2018). Trajectory tracking control for seafloor tracked vehicle by adaptive neural-fuzzy inference system Algorithm. *International Journal of Computers Communications & Control, 13*(4), 465–476.

Fan, Y., Zhang, Q. S., Wang, W. S., & Zhou, X. F. (2018). Speed regulation system of a flux-modulated permanent-magnet in-wheel motor based on sliding mode control and adaptive notch filter. *IEEE Transactions on Energy Conversion, 33*(4), 2183–2190.

Fukao, T., Nakagawa, H., & Adachi, N. (2000). Adaptive tracking control of a nonholonomic mobile robot. *IEE Transactions on Robotics and Automation, 16*(5), 609–615.

Huang, C., Naghdy, F., & Du, H. P. (2019). Fault tolerant sliding mode predictive control for uncertain steer-by-wire system. *IEE Transactions on Cybernetics, 49*(1), 261–272.

Jiang, W., Yan, Y., Yu, L. Q., Li, H. J., Du, L. Z., & Chen, W. (2018). Robust trajectory tracking control for parameter perturbation power cable mobile operation robot system. *Industrial Robot The International Journal of Robotics Research and Application, 45*(6), 744–757.

Jiao, J., Chen, J., Qiao, Y., Wang, W. Z., Wang, M. S., Chuan Gu, L., et al. (2018). Adaptive sliding mode control of trajectory tracking based on DC motor drive for agricultural tracked robot. *Journal of Agricultural Engineering, 34*(04), 64–70.

Jiao, J., Kong, W., Gu, L. C., Wang, Q., Gao, Y., & Yuan, C. C. (2015). Sliding parameter calculation of agricultural tracked robot based on UKF and SMO. *Journal of System Simulation, 27*(7), 1577–1583.

Kayacan, E., Ramon, H., & Saeys, W. (2012). Velocity control of a spherical rolling robot using a grey-PID type fuzzy controller with an adaptive step size. *IFAC Proceedings Volumes, 45*(22), 863–868.

Kayacan, E., Young, S. N., Peschel, J. M., & Chowdhary, G. (2018). High precision control of tracked field robots in the presence of unknown traction coefficients. *Journal of Field Robotics, 35*(7), 203–209.

Moreno-Valenzuela, J., Perez-Alcocer, R., Guerrero-Medina, M., & Dzul, A. (2018). Nonlinear PID-type controller for quadrotor trajectory tracking. *IEEE ASME Transactions on Mechatronics, 23*(5), 2436–2447.

Oberti, R., & Shapiro, A. (2016). Advances in robotic agriculture for crops. *Biosystems Engineering, 146*(Special Issue), 1–2.

Rios, H., Falcon, R., Gonzalez, O. A., & Dzul, A. (2019). Continuous sliding-mode control strategies for quadrotor robust tracking: Real-time application. *IEEE Transactions on Industrial Electronics, 66*(2), 1264–1272.

Taherkhorsandi, M., Mahmoodabadi, M. J., Talebipour, M., & Castillo-Villar, K. K. (2015). Pareto design of an adaptive robust hybrid of PID and sliding control for a biped robot via genetic algorithm optimization. *Nonlinear Dynamics, 79*(1), 251–263.

Wen, S. H., Chen, J. H., Qin, G. Q., Zhu, Q. G., & Wang, H. B. (2018). An improved fuzzy model predictive control algorithm based on the force/position control structure of the five-degree of freedom redundant actuation parallel robot. *International Journal of Advanced Robotic Systems, 15*(5). https://doi.org/10.1177/1729881418804979.

Xian, X. G. (2012). A development of H/W and S/W platform of remote controllable agricultural robot based on XP embedded system. *The Journal of The Korea Institute of Electronic Communication Sciences, 7*(5), 1125–1131.

Zhu, A.,B., Wang, B.,K., Tian, C., Zhang, H., & Chen, W. (2012). Dynamics modeling method and performance simulation for maneuvering system of tracked vehicle. *Joural of Machine Design National, 29*(9), 57–60.